Applied Physics Letters

Few-layer hexagonal boron nitride as a shield of brittle materials for cryogenic s-SNOM exploration of phonon polaritons

Cite as: Appl. Phys. Lett. **120**, 161101 (2022); https://doi.org/10.1063/5.0081203
Submitted: 07 December 2021 • Accepted: 01 April 2022 • Published Online: 19 April 2022

Debo Hu, Cheng Luo, Lixing Kang, et al.

Applied Physics Letters ARTICLE scitation.org/journal/apl

Few-layer hexagonal boron nitride as a shield of brittle materials for cryogenic s-SNOM exploration of phonon polaritons

Cite as: Appl. Phys. Lett. **120**, 161101 (2022); doi: 10.1063/5.0081203
Submitted: 7 December 2021 · Accepted: 1 April 2022 ·
Published Online: 19 April 2022

Debo Hu,[1] Cheng Luo,[1] Lixing Kang,[2] Mengkun Liu,[3] and Qing Dai[1,a)]

AFFILIATIONS

[1]CAS Key Laboratory of Nanophotonic Materials and Devices, CAS Key Laboratory of Standardization and Measurement for Nanotechnology, CAS Center for Excellence in Nanoscience, National Center for Nanoscience and Technology, Beijing 100190, China
[2]Suzhou Institute of Nano-Tech and Nano-Bionics, CAS, Suzhou 215123, China
[3]Department of Physics, Stony Brook University, Stony Brook, New York 11794, USA

Note: This paper is part of the APL Special Collection on Optical Nanoprobe Spectroscopy and Imaging.
[a)]**Author to whom correspondence should be addressed:** daiq@nanoctr.cn

ABSTRACT

Surface phonon polaritons (SPhPs) in van der Waals (vdW) materials are of great interest in fundamental and applied research fields. Probing the characteristics of vdW SPhPs at cryogenic temperatures is an essential task for their implementation in low-temperature physics. However, the most commonly used characterization technique of vdW SPhPs—scattering-type scanning near-field optical microscopy (s-SNOM) operating in a tapping mode (an intermittent-contact mode)—can be problematic at low temperatures because the sample being tested may become brittle and fragile. Therefore, high fracture toughness is desired for the samples under intermittent-contact s-SNOM scanning at low temperatures. In this work, by taking α-phase molybdenum trioxide (α-MoO_3) as an example, we first confirm the potential surface deterioration induced by tip-sample interactions at low temperatures. Then, we propose to use few-layer hexagonal boron nitride as a mechanically tough yet optically passive cladding layer to enhance the surface stability of α-MoO_3. Finally, we demonstrate the validity of our surface reinforcement strategy by probing the previously unexplored temperature dependence of SPhPs within the third Reststrahlen band of α-MoO_3. Our method allows a sustained operation of tapping mode s-SNOM at cryogenic temperatures with negligible effect on intrinsic properties of SPhPs.

Owing to the development of advanced characterization techniques like scattering-type scanning near-field optical microscopy (s-SNOM)[1–6] and the emergence of low-dimensional materials like van der Waals (vdW) crystals,[7–12] recently we have witnessed a renaissance of the research on surface phonon polaritons (SPhPs).[13–16] The hybrid photon–phonon nature of SPhPs[17] together with the intrinsic low-dimensional character of vdW materials[18–20] makes the associated electromagnetic energy extremely confined in space,[21,22] and therefore vdW SPhPs are a topic of intense current interest in both fundamental and technical research fields related to strong light–matter interactions.[23,24] Promising applications of vdW SPhPs include assisting the multiphoton spontaneous emission,[25] mediating the near-field and ballistic heat transfer,[26–28] enhancing the dynamical vacuum effects,[29] and improving the sensitivity of vibrational spectroscopy,[30,31] many of which involve cryogenic operating conditions.[28,32,33] Although cryogenic s-SNOM (cryo-SNOM) has been commercially available for several years[34,35] and graphene plasmon polaritons have been routinely probed by a couple of homebuilt cryo-SNOM systems,[36–41] reports on the near-field characterization of vdW SPhPs at cryogenic temperatures are rare.[42] This stems from specific difficulties in performing cryogenic nano-imaging of vdW SPhPs.

In this work, by taking biaxial α-phase molybdenum trioxide (α-MoO_3) as a representative, we first identify the surface deterioration of the microcrystal under investigation induced by tip-sample interactions at low temperatures as the main obstacle hindering the cryogenic nano-imaging of vdW SPhPs using a tapping mode s-SNOM. Then, we propose to use few-layer hexagonal boron nitride (*h*BN) as a mechanically tough yet optically passive cladding layer to enhance the

surface stability of α-MoO_3. Finally, we demonstrate the validity of our surface reinforcement strategy by probing the previously unexplored temperature dependence of SPhPs in the third Reststrahlen band (RB_3) of α-MoO_3.

s-SNOM operating in the tapping mode (the intermittent-contact mode) is not always noninvasive,[43,44] because there exists a time-varying (frequency $f \sim 270$ kHz) interaction force up to tens of nN (free amplitude $A \sim 100$ nm, 80% setpoint, cantilever force constant $k \sim 42$ N/m, quality factor of tip ~1000) between the vibrating tip and the sample surface,[45–47] which is equivalent to a high-rate stress on the order of GPa (Ref. 48) as a result of the tiny contact area and can potentially damage the surfaces of specific samples. This is especially the case at cryogenic temperatures, since many materials undergo a ductile-brittle transition when cooled down[49–52] and become more sensitive to the high-rate impact of the tip apex as a result of the deteriorated fracture toughness.[53,54] Considering previous first principles calculation has suggested the surface stability of α-MoO_3 is temperature dependent,[55] we chose α-MoO_3 as a model material for the experimental study of tip-induced surface deterioration at low temperatures and the corresponding protection strategy. Our imaging results obtained by a homebuilt cryo-SNOM system schematically illustrated in Fig. 1(a) (see Fig. S1 of the supplementary material for details inside the vacuum chamber) indeed indicate a reduced surface stability of α-MoO_3 at low temperatures. (Note that in all the experiments, we used Arrow^{TM} NCPt probes with their cantilevers micro-engineered. These processed probes exhibit comparable quality factors under vacuum-cryogenic conditions to those in ambient environment, thus, are nicknamed q_{Minus}.) A typical near-field optical image of bare α-MoO_3 microcrystals mechanically exfoliated onto SiO_2/Si substrates at 88 K is shown in Fig. 1(b), which indicates

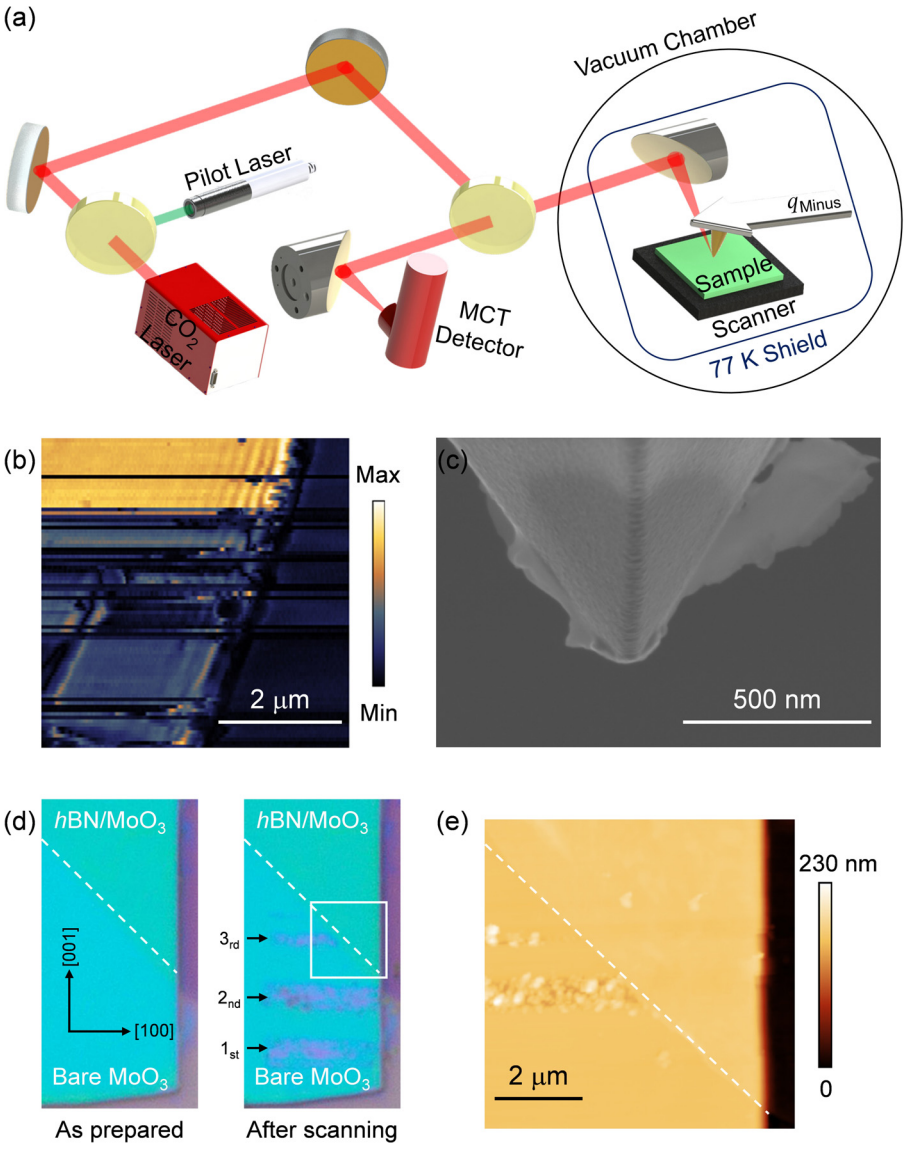

FIG. 1. (a) Schematics of the homebuilt cryo-SNOM system used in this work. (b) Near-field optical image indicating surface deterioration of bare α-MoO_3 induced by the tip-sample interaction at 88 K. (c) SEM image of the SNOM tip apex used in (b). (d) Optical images of a α-MoO_3 microcrystal partly cladded with a 5-nm-thick *h*BN flake before and after SNOM imaging at 88 K, the white dashed lines indicate the *h*BN boundary, the black arrows in the right panel indicate the scanning area in each round of the experiment, and the box marks the imaging area in (e). (e) AFM image of the partly cladded α-MoO_3 sample marked in (d) with the box.

the rapid surface deterioration of α-MoO_3 during cryo-SNOM scanning makes the imaging of SPhPs extremely difficult. (Such a problem has not been encountered under vacuum and room-temperature imaging conditions.) To find out what happened in the scanning process, we took a close look at the tip apex used in the experiment with the scanning electron microscope (SEM), and the image shown in Fig. 1(c) indicates that there is some flaky debris attaching to the tip apex. Therefore, we conjecture that a probable scenario for the imaging process of Fig. 1(b) is: first, the surface of α-MoO_3 became less stable as a result of low-temperature embrittlement and fractured under the repeated impact of the SNOM tip; then, some fragments of the broken surface adhered to the tip apex; finally, the deteriorated sample surface together with the contaminated tip-apex cause a significant decay of the near-field signal.

To solve the problem of surface deterioration and tip contamination in cryo-SNOM imaging, one has to resort to an appropriate cladding material that, on the one hand, can improve the mechanical toughness of the sample and, on the other hand, would not disturb optical imaging. Considering *h*BN exhibits a high fracture toughness, thus, is expected to be resistant to the impact of the tapping tip,[56] and its Reststrahlen bands are well-separated from those of α-MoO_3 (in the frequency range from 850 to 1200 cm^{-1}, the real parts of the in-plane and the out-of-plane dielectric constants of *h*BN are positive while the imaginary parts are relatively small as shown in Fig. S2 of the supplementary material),[57,58] we chose it to verify the validity of our surface reinforcement strategy. As shown in Fig. 1(d), we fabricated a α-MoO_3 sample partly cladded with a 5-nm-thick *h*BN flake using the standard dry transfer method[59] and put it into the trial of cryo-SNOM scanning at 88 K. Three rounds of scanning (along the [100] direction and cross the sample edge) have been conducted with the first two on the bare α-MoO_3 surface and the last one on the partly cladded sample surface. Without exception, all bare α-MoO_3 surface areas have been modified considerably by scanning, as seen from the comparison between the as-prepared and post-scanning sample optical micrographs. Only the *h*BN cladded site remained completely intact after scanning. Figure 1(e) shows the atomic force microscope (AFM) image corresponding to the third round scanning, and the direct contrast between the broken bare α-MoO_3 surface and the intact *h*BN-protected surface is strong evidence for the effectiveness of our surface reinforcement method.

To evaluate the optical consequences of *h*BN cladding, using the transfer-matrix method[60] and infrared dielectric parameters from Refs. 57, 58, and 61, we calculated and compared the phonon-polariton behaviors of a SiO_2/130-nm-thick α-MoO_3/vacuum structure and a SiO_2/130-nm-thick α-MoO_3/*h*BN/vacuum model system within RB_3 (960–1000 cm^{-1}) of α-MoO_3 with varying *h*BN

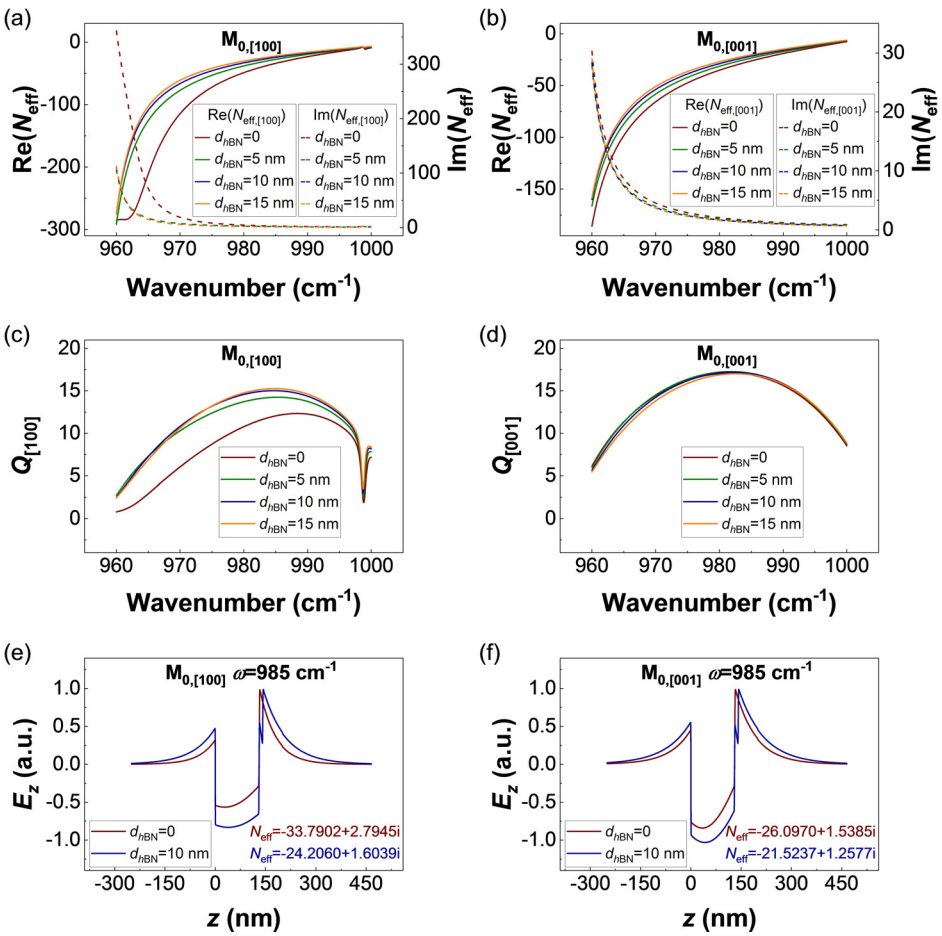

FIG. 2. (a) and (b) Calculated effective indices of refraction (N_{eff}) for the fundamental phonon-polariton modes in the SiO_2/α-MoO_3/*h*BN/vacuum structure with a fixed α-MoO_3 thickness of 130 nm and varying *h*BN thicknesses, propagating along the [100] ($M_{0,[100]}$) and [001] ($M_{0,[001]}$) crystalline directions of α-MoO_3 respectively. (c) and (d) *Q* factors of $M_{0,[100]}$ and $M_{0,[001]}$, respectively. (e) and (f) Electric field profiles of $M_{0,[100]}$ and $M_{0,[001]}$ at 985 cm^{-1} with/without a 10-nm-thick *h*BN cladding layer, respectively.

thicknesses. Figures 2(a) and 2(b) show the dispersions of the fundamental phonon-polariton modes of α-MoO_3 propagating along the [100] ($M_{0,[100]}$) and [001] ($M_{0,[001]}$) crystalline directions, respectively. It can be seen that both $M_{0,[100]}$ and $M_{0,[001]}$ are type I hyperbolic phonon-polariton modes with negative phase velocity (the negative real part of the effective indices of refraction N_{eff}) as a result of the negative out-of-plane dielectric constant of α-MoO_3 within RB_3[8,58] and suffer high propagation losses below the frequency 970 cm^{-1} (the large imaginary part of N_{eff}) resulting from the heavy damping of the nearby α-MoO_3 transverse optical phonon at 956.7 cm^{-1}.[58] Adding the *h*BN layer and increasing its thickness would generally compromise the field confinement factor (the absolute value of the real part of N_{eff}) while lowering the propagation loss at the same time (the decreasing imaginary part of N_{eff}). Specifically, in the case of $M_{0,[100]}$, the decrease in the propagation loss is more significant than that of the field confinement factor after *h*BN cladding, resulting in a net increase in the mode quality factor [$Q = |\mathrm{Re}(N_{eff})/\mathrm{Im}(N_{eff})|$] as shown in Fig. 2(c) (the sharp dips are due to the transverse optical phonon of α-MoO_3 at 998.7 cm^{-1}); in the case of $M_{0,[001]}$, the decreases of the real and imaginary parts of N_{eff} are almost proportional, leading to a *Q* factor nearly independent of *h*BN cladding as shown in Fig. 2(d). Since the *Q* factors of both $M_{0,[100]}$ and $M_{0,[001]}$ have their maximum values in the frequency range from 980 to 990 cm^{-1}, 985 cm^{-1} would be a preferred frequency in the following cryo-SNOM imaging experiments. To further assess the effect of *h*BN cladding on the excitation and detection of SPhPs at this selected frequency, we calculated the mode profiles (E_z components, with and without a 10-nm-thick *h*BN cladding layer) of $M_{0,[100]}$ and $M_{0.[001]}$, respectively, as shown in Figs. 2(e) and 2(f). Considering the *h*BN cladding layer only slightly modifies the mode profiles and the near-field imaging-related E_z components still extend well above the sample surface, our surface reinforcement method of *h*BN cladding would not impede cryo-SNOM imaging of α-MoO_3 SPhPs.

Next, we proceeded to the experimental verification of the performance of *h*BN cladding in cryo-SNOM imaging of SPhPs. To this end, we fabricated a sample on the SiO_2/Si substrate by cladding a 130-nm-thick α-MoO_3 microcrystal with a 10-nm-thick *h*BN flake. Thanks to the well-defined and mutually orthogonal boundaries of this α-MoO_3 crystal, we can probe its $M_{0,[100]}$ and $M_{0,[001]}$ modes simultaneously. In imaging of the $M_{0,[100]}$ ($M_{0,[001]}$) mode at 985 cm^{-1}, we scanned the sample along the [100] ([001]) direction and demodulated the near-field signal at the third-order harmonic of the tip-tapping frequency using a lock-in. (O_3, lower-order signals recorded simultaneously, usually exhibit inferior signal-to-noise ratio, as shown in Fig. S3 of the supplementary material.) As shown in Fig. 3(a), the sample surface survived the long-time high-rate impact of the SNOM tip and remained intact under the four different test temperatures. Interference fringes of both $M_{0,[100]}$ and $M_{0,[001]}$ caused by the

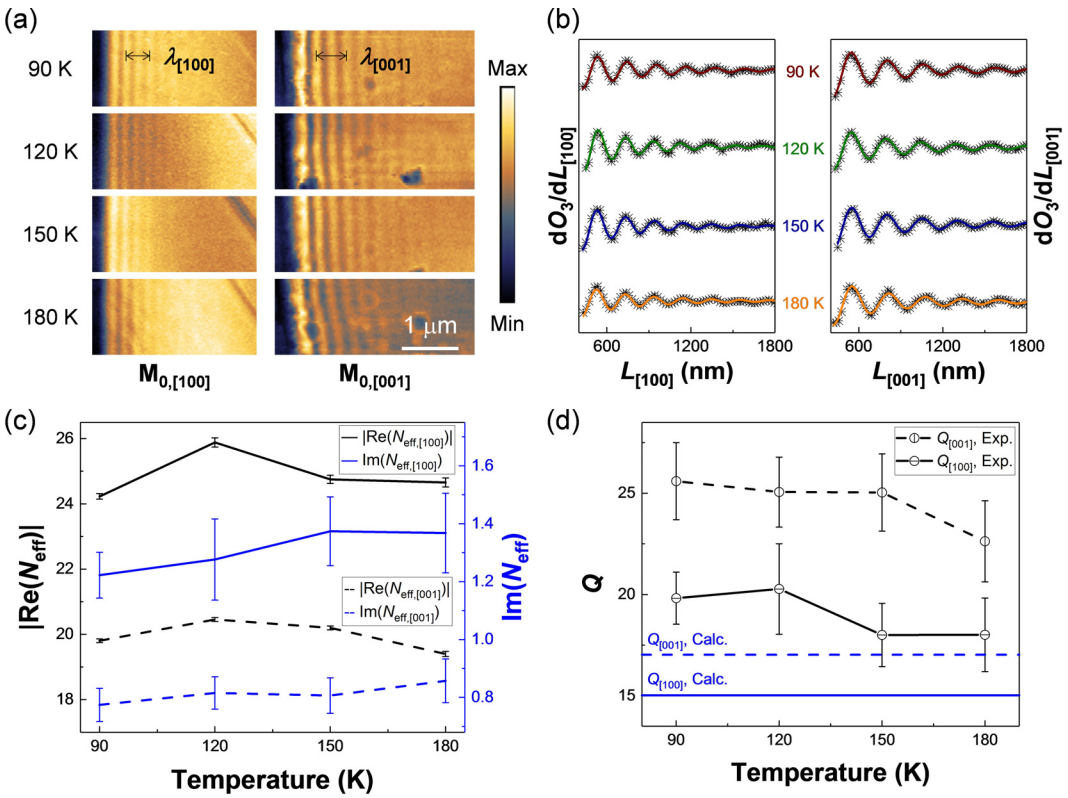

FIG. 3. (a) s-SNOM images of a 10-nm-thick *h*BN cladded 130-nm-thick α-MoO_3 microcrystal at cryogenic temperatures, along its [100] and [001] crystalline directions, respectively. (b) Fitting the experimental data with a damped sinusoidal waveform. (c) Fitted effective indices of refraction (N_{eff}) at different temperatures. (d) Fitted *Q* factors at different temperatures, dashed and solid horizontal lines indicate theoretically predicted room-temperature *Q* values for [001] and [100] directions, respectively. Bars in (c) and (d) denote standard deviations.

vectorial superposition of the tip-launched and the edge-reflected SPhPs can be easily distinguished in all near-field optical images (O_3) at different temperatures. To enhance the visibility of the interference fringes in Fig. 3(a) so as to facilitate the extraction of the propagation properties of both $M_{0,[100]}$ and $M_{0,[001]}$ at varying temperatures, we differentiated the images in Fig. 3(a) along the [100] ($dO_3/dL_{[100]}$) and [001] ($dO_3/dL_{[001]}$) directions, respectively, and left the nearest fringes to the sample edges out before fitting the processed data with a damped sinusoidal waveform. Because the damped sinusoidal waveform and its derivative exhibit the same damping factor and spatial frequency, the differentiation process would not negatively influence the accuracy of data fitting.[62] We can see in Fig. 3(b) that the processed experimental data fit very well with the damped sinusoidal waveform, and the extracted parameters from fitting for both $M_{0,[100]}$ and $M_{0,[001]}$ are illustrated in Figs. 3(c) and 3(d). As predicted by the theoretical calculations in Fig. 2, the $M_{0,[100]}$ mode indeed exhibits a more significant field confinement factor than that of $M_{0,[001]}$ while the $M_{0,[001]}$ mode holds a relatively higher Q factor, revealing the intrinsic in-plane optical anisotropy of α-MoO_3 across the entire temperature window explored. Thus far, the validity of our proposed surface reinforce method has been experimentally demonstrated, at least for α-MoO_3 on the most commonly used SiO_2/Si substrate. However, although the Q-temperature curves in Fig. 3(d) (see Fig. S4 of the supplementary material for results of a thicker sample) follow a similar trend with that of type II hyperbolic phonon polaritons in bare α-MoO_3,[42] and the observed low-temperature Q factors are indeed larger than the theoretically predicted room-temperature ones, the wave-guiding properties of type I hyperbolic phonon polaritons in *h*BN cladded α-MoO_3 do show slight non-monotonic temperature dependence within the investigated temperature range in our cryo-SNOM experiments. This non-monotonity might originate from the non-trivial strain imposed by the *h*BN cladding layer,[63] as evidenced by the different temperature dependence of the Raman spectrum of bare and cladded α-MoO_3 shown in Fig. S5 of the supplementary material.

To date, cryo-SNOM remains one of a few diffraction-unlimited techniques which can probe the nanoscale electrodynamics of vdW crystals or other quantum materials at low temperatures.[64–67] Surface deterioration of samples under cryo-SNOM test induced by tip-sample interactions is an aspect not discussed before. We first raise awareness of this problem and propose and verify an effective way of bypassing this obstacle in this work via *h*BN cladding. Using this method, we reveal the temperature dependence of the waveguiding properties of type I hyperbolic phonon polaritons within RB_3 of α-MoO_3. Our method allows a sustained operation of tapping mode s-SNOM at cryogenic temperatures with negligible effect on the intrinsic properties of the sample which thus can be adopted as a standard method and used in the imaging of other polaritons, like surface exciton polaritons,[68–70] Cooper pair polaritons,[71] and surface magnon polaritons[72–74] at low temperatures. Aside from that, s-SNOM imaging of brittle materials at ambient temperatures can also benefit from this method.

See the supplementary material for a description of the cryo-SNOM assembly inside the vacuum chamber, an explanation about the applicable frequency range of the *h*BN protection layer, a comparison between the second- and third-harmonic demodulated images, the experimental results of a thicker α-MoO_3 sample, and the low-temperature Raman measurements results.

Q.D. acknowledges the support from the National Natural Science Foundation of China (Grant No. 51925203). D.H. acknowledges the support from the National Natural Science Foundation of China (Grant No. 52072083) and the Youth Innovation Promotion Association, CAS. Building of the cryo-SNOM used in this work was supported by the CAS Scientific Equipment Development Project and we acknowledge the technical support from Ithatron Instruments. D.H. acknowledges Professor S. P. Sun for the communications about MoO_3 surface stability, Professor M. X. Liu and Professor G. J. Zhang for the discussions on tip-sample interactions, and Dr. S. C. Sun for the help in low-temperature Raman measurements.

AUTHOR DECLARATIONS

Conflict of Interest

The authors have no conflicts to disclose.

DATA AVAILABILITY

The data that support the findings of this study are available from the corresponding author upon reasonable request.

REFERENCES

[1]F. Keilmann, J. Microsc. **194**, 567 (1999).
[2]A. Huber, N. Ocelic, D. Kazantsev, and R. Hillenbrand, Appl. Phys. Lett. **87**, 081103 (2005).
[3]A. J. Huber, B. Deutsch, L. Novotny, and R. Hillenbrand, Appl. Phys. Lett. **92**, 203104 (2008).
[4]A. J. Huber, N. Ocelic, and R. Hillenbrand, J. Microsc. **229**, 389 (2008).
[5]X. Chen, D. Hu, R. Mescall, G. You, D. N. Basov, Q. Dai, and M. Liu, Adv. Mater. **31**, 1804774 (2019).
[6]W. Ma, G. Hu, D. Hu, R. Chen, T. Sun, X. Zhang, Q. Dai, Y. Zeng, A. Alù, C. Qiu, and P. Li, Nature **596**, 362 (2021).
[7]S. Dai, Z. Fei, Q. Ma, A. S. Rodin, M. Wagner, A. S. McLeod, M. K. Liu, W. Gannett, W. Regan, K. Watanabe, T. Taniguchi, M. Thiemens, G. Dominguez, A. H. C. Neto, A. Zettl, F. Keilmann, P. Jarillo-Herrero, M. M. Fogler, and D. N. Basov, Science **343**, 1125 (2014).
[8]E. Yoxall, M. Schnell, A. Y. Nikitin, O. Txoperena, A. Woessner, M. B. Lundeberg, F. Casanova, L. E. Hueso, F. H. L. Koppens, and R. Hillenbrand, Nat. Photonics **9**, 674 (2015).
[9]P. Li, I. Dolado, F. J. Alfaro-Mozaz, F. Casanova, L. E. Hueso, S. Liu, J. H. Edgar, A. Y. Nikitin, S. Vélez, and R. Hillenbrand, Science **359**, 892 (2018).
[10]W. Ma, P. Alonso-González, S. Li, A. Y. Nikitin, J. Yuan, J. Martín-Sánchez, J. Taboada-Gutiérrez, I. Amenabar, P. Li, S. Vélez, C. Tollan, Z. Dai, Y. Zhang, S. Sriram, K. Kalantar-Zadeh, S. Lee, R. Hillenbrand, and Q. Bao, Nature **562**, 557 (2018).
[11]Z. Zheng, N. Xu, S. L. Oscurato, M. Tamagnone, F. Sun, Y. Jiang, Y. Ke, J. Chen, W. Huang, W. L. Wilson, A. Ambrosio, S. Deng, and H. Chen, Sci. Adv. **5**, v8690 (2019).
[12]J. Taboada-Gutiérrez, G. Álvarez-Pérez, J. Duan, W. Ma, K. Crowley, I. Prieto, A. Bylinkin, M. Autore, H. Volkova, K. Kimura, T. Kimura, M. H. Berger, S. Li, Q. Bao, X. P. A. Gao, I. Errea, A. Y. Nikitin, R. Hillenbrand, J. Martín-Sánchez, and P. Alonso-González, Nat. Mater. **19**, 964 (2020).
[13]J. D. Caldwell, L. Lindsay, V. Giannini, I. Vurgaftman, T. L. Reinecke, S. A. Maier, and O. J. Glembocki, Nanophotonics **4**, 44 (2015).
[14]D. N. Basov, M. M. Fogler, and F. J. García De Abajo, Science **354**, g1992 (2016).
[15]T. Low, A. Chaves, J. D. Caldwell, A. Kumar, N. X. Fang, P. Avouris, T. F. Heinz, F. Guinea, L. Martin-Moreno, and F. Koppens, Nat. Mater. **16**, 182 (2017).
[16]J. D. Caldwell, I. Aharonovich, G. Cassabois, J. H. Edgar, B. Gil, and D. N. Basov, Nat. Rev. Mater. **4**, 552 (2019).
[17]D. N. Basov, A. Asenjo-Garcia, P. J. Schuck, X. Zhu, and A. Rubio, Nanophotonics **10**, 549 (2021).
[18]K. S. Novoselov, D. Jiang, F. Schedin, T. J. Booth, V. V. Khotkevich, S. V. Morozov, and A. K. Geim, Proc. Natl. Acad. Sci. U. S. A. **102**, 10451 (2005).

[19]A. K. Geim and I. V. Grigorieva, Nature **499**, 419 (2013).
[20]K. S. Novoselov, A. Mishchenko, A. Carvalho, and A. H. Castro Neto, Science **353**, 461 (2016).
[21]S. Dai, W. Fang, N. Rivera, Y. Stehle, B. Jiang, J. Shen, R. Y. Tay, C. J. Ciccarino, Q. Ma, D. Rodan-Legrain, P. Jarillo-Herrero, E. H. T. Teo, M. M. Fogler, P. Narang, J. Kong, and D. N. Basov, Adv. Mater. **31**, 1806603 (2019).
[22]N. Li, X. Guo, X. Yang, R. Qi, T. Qiao, Y. Li, R. Shi, Y. Li, K. Liu, Z. Xu, L. Liu, F. J. García De Abajo, Q. Dai, E. Wang, and P. Gao, Nat. Mater. **20**, 43 (2021).
[23]N. Rivera, T. Christensen, and P. Narang, Nano Lett. **19**, 2653 (2019).
[24]N. Rivera and I. Kaminer, Nat. Rev. Phys. **2**, 538 (2020).
[25]N. Rivera, G. Rosolen, J. D. Joannopoulos, I. Kaminer, and M. Soljačić, Proc. Natl. Acad. Sci. U. S. A. **114**, 13607 (2017).
[26]B. Song, A. Fiorino, E. Meyhofer, and P. Reddy, AIP Adv. **5**, 53503 (2015).
[27]B. Zhao, B. Guizal, Z. M. Zhang, S. Fan, and M. Antezza, Phys. Rev. B **95**, 245437 (2017).
[28]S. Huberman, R. A. Duncan, K. Chen, B. Song, V. Chiloyan, Z. Ding, A. A. Maznev, G. Chen, and K. A. Nelson, Science **364**, 375 (2019).
[29]J. Sloan, N. Rivera, J. D. Joannopoulos, and M. Soljačić, Phys. Rev. Lett. **127**, 53603 (2021).
[30]M. Autore, P. Li, I. Dolado, F. J. Alfaro-Mozaz, R. Esteban, A. Atxabal, F. Casanova, L. E. Hueso, P. Alonso-González, J. Aizpurua, A. Y. Nikitin, S. Vélez, and R. Hillenbrand, Light **7**, 17172 (2018).
[31]A. Bylinkin, M. Schnell, M. Autore, F. Calavalle, P. Li, J. Taboada-Gutièrrez, S. Liu, J. H. Edgar, F. Casanova, L. E. Hueso, P. Alonso-Gonzalez, A. Y. Nikitin, and R. Hillenbrand, Nat. Photonics **15**, 197 (2021).
[32]G. Plunien, R. Schützhold, and G. Soff, Phys. Rev. Lett. **84**, 1882 (2000).
[33]C. M. Wilson, G. Johansson, A. Pourkabirian, M. Simoen, J. R. Johansson, T. Duty, F. Nori, and P. Delsing, Nature **479**, 376 (2011).
[34]T. Gokus, A. Huber, and M. Eisele, paper presented at the 2018 Conference on Lasers and Electro-Optics (CLEO), San Jose, CA, USA, 2018.
[35]W. Luo, M. Boselli, J. Poumirol, I. Ardizzone, J. Teyssier, D. van der Marel, S. Gariglio, J. Triscone, and A. B. Kuzmenko, Nat. Commun. **10**, 2774 (2019).
[36]H. U. Yang, E. Hebestreit, E. E. Josberger, and M. B. Raschke, Rev. Sci. Instrum. **84**, 23701 (2013).
[37]G. X. Ni, A. S. McLeod, Z. Sun, L. Wang, L. Xiong, K. W. Post, S. S. Sunku, B. Y. Jiang, J. Hone, C. R. Dean, M. M. Fogler, and D. N. Basov, Nature **557**, 530 (2018).
[38]D. J. Rizzo, B. S. Jessen, Z. Sun, F. L. Ruta, J. Zhang, J. Yan, L. Xian, A. S. McLeod, M. E. Berkowitz, K. Watanabe, T. Taniguchi, S. E. Nagler, D. G. Mandrus, A. Rubio, M. M. Fogler, A. J. Millis, J. C. Hone, C. R. Dean, and D. N. Basov, Nano Lett. **20**, 8438 (2020).
[39]W. Zhao, H. Li, X. Xiao, Y. Jiang, K. Watanabe, T. Taniguchi, A. Zettl, and F. Wang, Nano Lett. **21**, 3106 (2021).
[40]Y. Dong, L. Xiong, I. Y. Phinney, Z. Sun, R. Jing, A. S. McLeod, S. Zhang, S. Liu, F. L. Ruta, H. Gao, Z. Dong, R. Pan, J. H. Edgar, P. Jarillo-Herrero, L. S. Levitov, A. J. Millis, M. M. Fogler, D. A. Bandurin, and D. N. Basov, Nature **594**, 513 (2021).
[41]W. Zhao, S. Zhao, H. Li, S. Wang, S. Wang, M. I. B. Utama, S. Kahn, Y. Jiang, X. Xiao, S. Yoo, K. Watanabe, T. Taniguchi, A. Zettl, and F. Wang, Nature **594**, 517 (2021).
[42]G. Ni, A. S. McLeod, Z. Sun, J. R. Matson, C. F. B. Lo, D. A. Rhodes, F. L. Ruta, S. L. Moore, R. A. Vitalone, R. Cusco, L. Artus, L. Xiong, C. R. Dean, J. C. Hone, A. J. Millis, M. M. Fogler, J. H. Edgar, J. D. Caldwell, and D. N. Basov, Nano Lett. **21**, 5767 (2021).
[43]M. Yu, T. Kowalewski, and R. S. Ruoff, Phys. Rev. Lett. **85**, 1456 (2000).
[44]K. Bian, C. Gerber, A. J. Heinrich, D. J. Müller, S. Scheuring, and Y. Jiang, Nat. Rev. Methods Primers **1**, 36 (2021).
[45]R. García and A. San Paulo, Phys. Rev. B **60**, 4961 (1999).
[46]S. C. Fain, K. A. Barry, M. G. Bush, B. Pittenger, and R. N. Louie, Appl. Phys. Lett. **76**, 930 (2000).
[47]S. Hu and A. Raman, Appl. Phys. Lett. **91**, 123106 (2007).
[48]O. P. Behrend, F. Oulevey, D. Gourdon, E. Dupas, A. J. Kulik, G. Gremaud, and N. A. Burnham, Appl. Phys. A **66**, S219 (1998).
[49]A. W. Magnusson and W. M. Baldwin, J. Mech. Phys. Solids **5**, 172 (1957).
[50]D. A. Wigley, *Mechanical Properties of Materials at Low Temperatures* (Springer, Boston, 1971).
[51]A. Lupinacci, J. Kacher, A. A. Shapiro, P. Hosemann, and A. M. Minor, J. Mater. Res. **36**, 1751 (2021).
[52]H. Kim and S. Roberts, J. Am. Ceram. Soc. **77**, 3099 (1994).
[53]K. S. Chan, Metall. Mater. Trans. A **34**, 2315 (2003).
[54]E. Frutos, J. L. González-Carrasco, and T. Polcar, J. Eur. Ceram. Soc. **36**, 3235 (2016).
[55]S. P. Sun, J. L. Zhu, S. Gu, X. P. Li, W. N. Lei, Y. Jiang, D. Q. Yi, and G. H. Chen, Appl. Surf. Sci. **467–468**, 753 (2019).
[56]Y. Yang, Z. Song, G. Lu, Q. Zhang, B. Zhang, B. Ni, C. Wang, X. Li, L. Gu, X. Xie, H. Gao, and J. Lou, Nature **594**, 57 (2021).
[57]C. H. Perry, G. Rupprecht, and R. Geick, Phys. Rev. **146**, 543 (1966).
[58]G. Álvarez-Pérez, T. G. Folland, I. Errea, J. Taboada-Gutiérrez, J. Duan, J. Martín-Sánchez, A. I. F. Tresguerres-Mata, J. R. Matson, A. Bylinkin, M. He, W. Ma, Q. Bao, J. I. Martín, J. D. Caldwell, A. Y. Nikitin, and P. Alonso-González, Adv. Mater. **32**, 1908176 (2020).
[59]L. Wang, I. Meric, P. Y. Huang, Q. Gao, Y. Gao, H. Tran, T. Taniguchi, K. Watanabe, L. M. Campos, D. A. Muller, J. Guo, P. Kim, J. Hone, K. L. Shepard, and C. R. Dean, Science **342**, 614 (2013).
[60]N. C. Passler and A. Paarmann, J. Opt. Soc. Am. B **34**, 2128 (2017).
[61]J. Kischkat, S. Peters, B. Gruska, M. Semtsiv, M. Chashnikova, M. Klinkmüller, O. Fedosenko, S. Machulik, A. Aleksandrova, G. Monastyrskyi, Y. Flores, and W. Ted Masselink, Appl. Opt. **51**, 6789 (2012).
[62]G. X. Ni, L. Wang, M. D. Goldflam, M. Wagner, Z. Fei, A. S. McLeod, M. K. Liu, F. Keilmann, B. Özyilmaz, A. H. C. Neto, J. Hone, M. M. Fogler, and D. N. Basov, Nat. Photonics **10**, 244 (2016).
[63]X. Sun, J. Shi, M. A. Washington, and T. Lu, Appl. Phys. Lett. **111**, 151603 (2017).
[64]H. F. Hess, E. Betzig, T. D. Harris, L. N. Pfeiffer, and K. W. West, Science **264**, 1740 (1994).
[65]J. M. Atkin, S. Berweger, A. C. Jones, and M. B. Raschke, Adv. Phys. **61**, 745 (2012).
[66]M. Liu, A. J. Sternbach, and D. N. Basov, Rep. Prog. Phys. **80**, 014501 (2017).
[67]A. Tomadin, A. Principi, J. C. W. Song, L. S. Levitov, and M. Polini, Phys. Rev. Lett. **115**, 87401 (2015).
[68]J. Lagois and B. Fischer, Phys. Rev. Lett. **36**, 680 (1976).
[69]F. DeMartini, M. Colocci, S. E. Kohn, and Y. R. Shen, Phys. Rev. Lett. **38**, 1223 (1977).
[70]L. Schultheis and J. Lagois, Solid State Commun. **44**, 1557 (1982).
[71]M. E. Berkowitz, B. S. Y. Kim, G. Ni, A. S. McLeod, C. F. B. Lo, Z. Sun, G. Gu, K. Watanabe, T. Taniguchi, A. J. Millis, J. C. Hone, M. M. Fogler, R. D. Averitt, and D. N. Basov, Nano Lett. **21**, 308 (2021).
[72]R. Macêdo and R. E. Camley, Phys. Rev. B **99**, 14437 (2019).
[73]J. Sloan, N. Rivera, J. D. Joannopoulos, I. Kaminer, and M. Soljačić, Phys. Rev. B **100**, 235453 (2019).
[74]P. Sivarajah, A. Steinbacher, B. Dastrup, J. Lu, M. Xiang, W. Ren, S. Kamba, S. Cao, and K. A. Nelson, J. Appl. Phys. **125**, 213103 (2019).